Korean J. Chem. Eng., 35(1), 61-72 (2018)
DOI: 10.1007/s11814-017-0266-z

pISSN: 0256-1115
eISSN: 1975-7220

Gas-liquid mass transfer studies: The influence of single- and double-impeller configurations in stirred tanks

Ao Pan*, Minghui Xie, Jianye Xia*,†, Ju Chu*, and Yingping Zhuang*,†**

*State Key Laboratory of Bioreactor Engineering, East China University of Science & Technology P. O. Box 329, 130 Meilong Road, Shanghai 200237 P. R. China
**Wenzhou Great Wall Mixer Design Institute, Wenzhou, Zhejiang 325019, China
(*Received 22 July 2017 • accepted 21 September 2017*)

Abstract-The influence of impeller structure on the mass transfer characteristics was studied with the steady-state method for gas-liquid volumetric mass transfer coefficient (k_La). The single-impeller configurations included eight impeller types (three radial flow impellers, four axial flow impellers and one mixed flow impeller), and the double-impeller included three configurations (RT+RT, RT+WH_D, WH_D+WH_D). For single-impeller, the gas-liquid mass transfer rates of radial flow impellers were better than those of axial flow impellers under the same rotation speed and gas flow rate. The mass transfer performance (defined as the volumetric mass transfer coefficient per unit power input) of radial flow impellers were also better than that of axial flow impellers. With the same k_La value under a certain gas flow rate, the local bubble size distribution between radial flow impeller and axial flow impeller was similar. As for double impellers, RT+RT provided the highest mass transfer rate under certain rotation speed and gas flow rate, while WH_D+WH_D gave the highest values of gas-liquid mass transfer coefficient with the same power consumption.

Keywords: Gas-liquid System, Gas-liquid Mass Transfer Correlations, Radial and Axial Impellers, Impeller Mass Transfer Performance, Bubble Size Distribution

INTRODUCTION

Mechanically stirred gas-liquid tanks are widely used in chemical, food and biochemical processes. In many chemical and biochemical gas-liquid reaction processes, interphase mass transfer rate is always the limiting step for reaction rate. The mass transfer rate is an important parameter for judging the impeller system capacity. The designs and schemes of impeller system must be investigated to enhance gas-liquid mass transfer rate and mass transfer performance (defined as the volumetric mass transfer coefficient per unit power input).

The following authors compared the mass transfer rate and mass transfer performance of various impeller configurations. For single-impeller configurations, van't Riet [1] collected the literature data of impeller specific power consumption and superficial gas velocity to summarize them into equations for predicting mass transfer coefficient of single impeller, regardless of impeller type. Some authors also believe that the shape of the impeller has nothing to do with the mass transfer performance [2-5]. On the other hand, others believe the influence of single-impeller configuration on the mass transfer capacity cannot be neglected. Warmoeskerken and Smith [6] found that the Rushton turbine produces lower k_La values than the hollow blade turbine. On the contrary, higher k_La data for Rushton turbine compared to hollow blade turbine found Linek, Benes, and Sinkule [7]. Martin [8] and Martin, Mc Farlane, and Nienow [9] showing that the k_La values of axial flow impellers "Prochem Maxflo T" are 30% lower than those measured with Rushton turbine at the same power consumption. Chen et al. [10] found that slightly better performance was achieved by using concave-blade and comb-blade than Rushton impeller with identical power input and superficial gas velocity in the air-water system. Zhu et al. [11] found radial flow impellers produce slightly higher mass transfer rate than axial flow impellers. Whereas Sardeing et al. [12] used the overall transfer efficiency to judge the performance of single impellers and found that axial impellers perform better than the radial flow impellers.

For multiple-impeller configurations, Bouaifi and Roustan [13] found the same k_La data for various double-impeller configurations at the same energy consumption. Moucha et al. [14] found the impeller configurations with high power number provide better mass transfer performance. Moucha et al. [15] concluded that radial flow impellers provide higher (20% up to 50%) mass transfer coefficients than the axial flow impellers in the air-water system, and the combined configuration of an RT impeller in the bottom and two axial impellers in the upper sections does not achieve the mass transfer performance of 3RT. Shewale and Pandit [16] found 3PBTD performs better in mass transfer ability than 2PBTD-DT with high power input, while reverse trend found under low power input. Ungerman and Heindel [17] found that the dual Rushton-type impeller scheme exhibits the highest volumetric mass transfer rates for all operating conditions; however, it also displays the lowest mass transfer performance for all conditions due to its high power consumption. Fujasová et al. [18] found that 3RT, RT+2PBD and RT+2PBU are the most efficient impeller combinations for the

†To whom correspondence should be addressed.
E-mail: jyxia@ecust.edu.cn, ypzhuang@ecust.edu.cn

mass transfer performance in the triple-impeller vessel. Xie et al. [19] used six impeller combinations to study the average volumetric mass transfer coefficient. It showed that the axial flow impellers have a better mass transfer performance than the radial flow impellers under superficial gas velocity of 1.625 mm/s and 8.124 mm/s with the same power input. Buffo et al. [20] investigated mass transfer efficiency (k_La/P) of seven different dual-impeller configurations in a stirred tank bioreactor. It was found that EEDP-EEUP, RT-EEDP and EEDP-RT combinations gave a mass transfer efficiency up to 5.09 J^{-1}, which was 87% higher than for the RT-RT combination.

It is apparent from this overview that the conclusions about the influence of impeller configurations on the mass transfer capacity are still equivocal. This is partially caused by the different methods used for the k_La data evaluation. The methods used for the determination of the volumetric mass transfer coefficient can be divided into two classes: dynamic ($dC/dt\neq0$) and steady-state ($dC/dt=0$). The dynamic methods derive the k_La value from a concentration step change of a soluble gas component in the inlet gas stream, while the steady-state methods employ a chemical reaction to induce a constant concentration in the liquid phase above or below saturation. Most of the conclusions mentioned above were obtained by the dynamic methods. As for dynamic methods, the flow behavior of the gas phase may significantly affect the results. Heijnen et al. [21] found that in viscous gas-liquid system, tiny bubbles (d<1 mm), which occupy some fraction of the gas hold up, lead to considerable bias on measured k_La value by using the dynamic method. Linek et al. [22] compared the steady-state methods and dynamic methods, finding that some of the dynamic methods give underestimated k_La than that of steady-state method compared to experimental results. The only case in which there is no need to resort to models for the behavior of the gas phase is when a pure gas is absorbed in a completely de-gassed liquid [23]. A way to obtain this is to evacuate the system under agitation in order to desorb all the dissolved gasses (nitrogen and oxygen) and then absorb pure oxygen, and the k_La value obtained does certainly coincide with the real value. The dynamic methods are also used for high demand. To get more accurate results using this method, oxygen probes with high response sensitivity are required, and unsteady saturated dissolved oxygen concentration under aeration should

Table 1. Configuration data of tank

	Single-impeller configuration	Double-impeller configuration
Tank diameter, D_t (m)	0.48	0.48
Impeller diameter, D_{im} (m)	0.2	0.2
Liquid height, H_l (m)	0.52	0.52
Baffle width, B (m)	0.04	0.04
Sparger diameter, D_{sp} (m)	0.012	0.012
Bottom clearance of sparger, C_{sp} (m)	0.08	0.08
Impeller spacing, ΔC (m)		0.2
Bottom clearance of impeller (m)	C_s=0.15	C_d=0.12
Oxygen probe clearance, P_b (m)	0.2	0.2
Wall distance of probe, P_w (m)	0.12	0.12

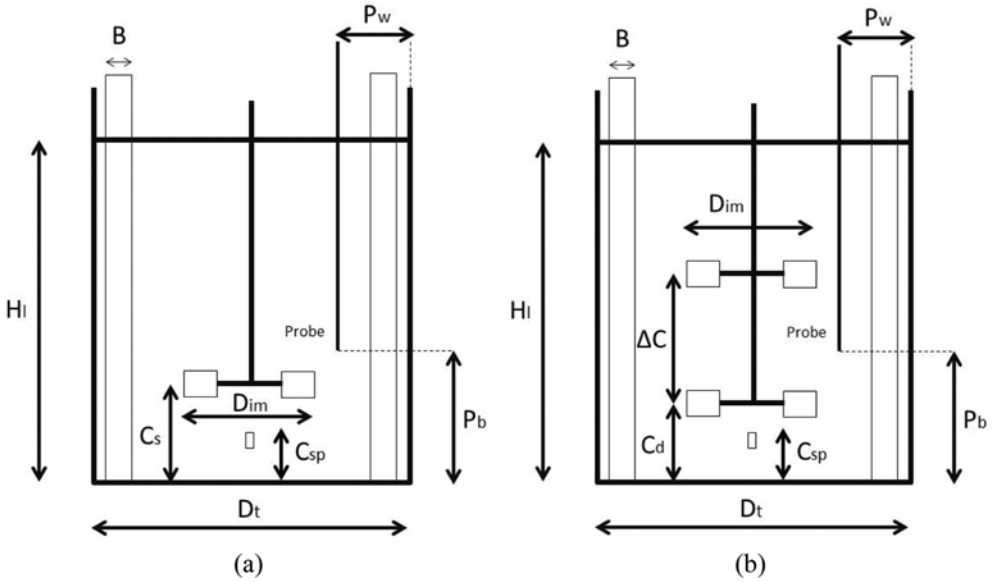

Fig. 1. Tank configurations: (a) Single-impeller configuration; (b) double-impeller configuration.

be considered. The steady-state methods are regarded as being less prone to the gas phase behavior [24], and have no need for high sensitivity to dissolved oxygen probes and consideration of changes of saturated dissolved oxygen concentration.

In this study, we used the steady-state sulfite method to measure the volume mass transfer rate. The mass transfer rate and mass transfer performance of various single- and double-impeller configurations were investigated in a stirred tank reactor. The mass transfer correlated empirical equations for single- and double-impeller configurations were done. Local bubble size distribution of different single-impellers with similar mass transfer rate was also compared and interpreted by relating it to the k_La distribution discrepancies between impellers.

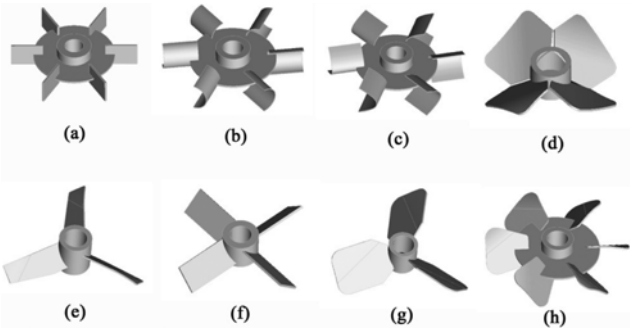

Fig. 2. Impellers used in this article ((a) RT, (b) HCDT, (c) PDT, (d) WH_{DU}, (e) CBY_N, (f) PBT, (g) WH_D, (h) HDT).

EXPERIMENT MATERIAL AND METHOD

1. Experimental Setup

The experiments were in a flat-bottom cylindrical vessel with internal diameter (D_t) of 0.48 m. The initial liquid volume (V) was 0.094 m^3 and corresponding liquid height (H_l) was 0.52 m. The tank was equipped with four vertical baffles (0.04 m in width (B) and 0.01 m in thickness). The clearance between wall and baffle was 0.01 m. The configurations of single- and double-impeller were studied in the experiments. Dimension details for the two setups can be found in Table 1 and Fig. 1. The impeller clearance ($0.3D_t$) in the single-impeller configuration was set a little higher than the clearance of bottom-impeller ($0.25D_t$) in the double-impeller configuration, so that mixing effect of upper part in the tank would be better. Tube sparger with internal diameter of 0.012 m was located 0.08 m above the tank bottom.

Eight different impellers were investigated in the experiments (Fig. 2). Among them, the Rushton turbine (RT), half-circular-blade disk turbine (HCDT) and parabolic-blade disk turbine (PDT) are radial impellers; three-narrow-blade hydrofoil impeller (CBY_N), 45° pitched blade turbine (PBT), three-wide-blade hydrofoil impeller pumping down (WH_D) and hydrofoil-blade disk turbine (HDT) are axial impellers; and wide-blade hydrofoil impeller with two pumping down blades and two pumping up blades (WH_{DU}) is a mixed flow impeller. RT+RT (bottom impeller+upper impeller, the same for the following), RT+WH_D and WH_D+WH_D were chosen to investigate as double-impeller setups.

The experiments were performed under room temperature of 25±1 °C and atmospheric pressure. Tap water was used as the working fluid and air was injected into the tank through a sparger. Impeller rotation speed in this work was in the range from 100 rpm to 300 rpm. Gas flow rate was set in the range from 0.33 (L/s) to 2.82 (L/s), corresponding to 0.2 vvm to 1.8 vvm.

2. The Steady-state Method for Measuring the k_La

The steady-state sulfite method was employed for the mass transfer measurement in this work [25]. The method relies on an immediate chemical reaction in the liquid. The chemical reaction is that with Cu^{2+} as the catalyzer in the liquid, sodium sulfite can be oxidized to sodium sulfate immediately by the dissolved oxygen. The chemical reaction is shown below:

$$2Na_2SO_3 + O_2 \xrightarrow{Cu^{2+}} 2Na_2SO_4$$

The tank was operated under continuous mode by continuously feeding sodium sulfite solution into the tank. As shown in Fig. 3(a), the first bottle of Na_2SO_3 solution with a concentration of 500 mol/m^3 was used to absorb the oxygen in the air to eliminate any variation of Na_2SO_3 concentration in the second bottle. The Na_2SO_3 solution with a concentration of 50 mol/m^3 in the second bottle was fed into the tank by a peristaltic pump. The concentration of Na_2SO_4 solution in the stirred tank was kept below 2 mol/m^3

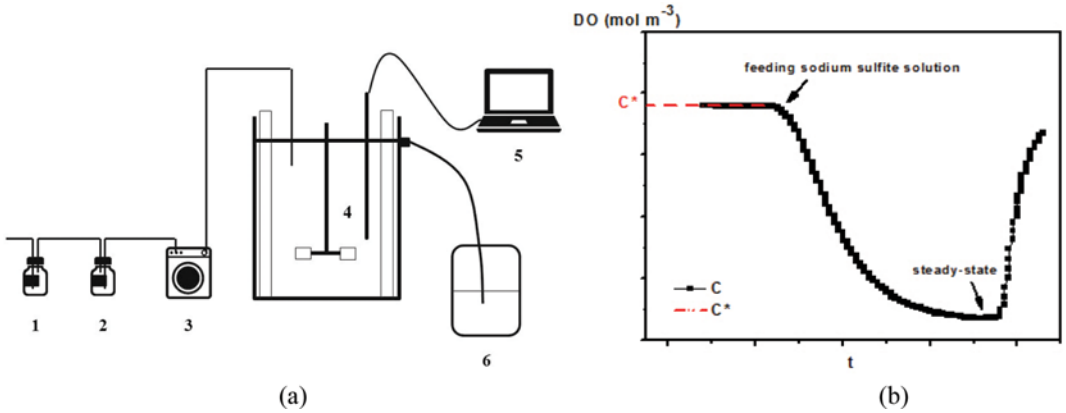

Fig. 3. (a) Experiment setup: (1) 1st bottle of Na_2SO_3, (2) 2nd bottle of Na_2SO_3, (3) peristaltic pump, (4) dissolved oxygen probe, (5) computer, (6) overflow device. (b) Dissolved change during experiments.

Table 2. Data for mass transfer correlations fitting

Impeller type	Single-axial impeller	Single-radial impeller	RT+RT	RT+WH_D	WH_D+WH_D
Corresponding equation	Eq. (8)	Eq. (9)	Eq. (10)	Eq. (11)	Eq. (12)
Impeller included	CBY_N, PBT, WH_D, HDT	RT, HCDT, PDT	RT	RT, WH_D	WH_D
Number of points	31	39	15	15	12
Range of P/V (W m^{-3})	65-593	41-1891	87-2923	80-1540	50-1226
Range of u_g (m/s)	0.00185-0.01563				
R^2	0.93	0.98	0.98	0.97	0.96

during all the experiments.

Meanwhile, dissolved oxygen (DO) was detected using the dissolved oxygen probe (InPro6800, METTLER-TOLEDO, Switzerland). The detailed position of the dissolved oxygen probe is shown in Table 1 and Fig. 1. The change of dissolved oxygen during the experiments is shown in Fig. 3(b). When dissolved oxygen reached saturation, sodium sulfite solution was fed into water and dissolved oxygen began to decrease. If DO level did not change with time, it was assumed to be steady state. At steady state, oxygen consumption rate by the reaction equals to the interphase oxygen transfer rate.

The measurement method is based on Eq. (1):

$$\frac{dC}{dt} = k_L a(C^* - C) - r \quad (1)$$

In Eq. (1), k_La is the volume mass transfer coefficient (s^{-1}); C^* is the dissolved oxygen concentration at saturation (mol/m^3); C is the dissolved oxygen concentration (mol/m^3); r is the oxygen consumption rate ($mol \cdot m^{-3} \cdot s^{-1}$) and calculated by Eq. (2).

$$r = QM/2V \quad (2)$$

where Q is the feed rate of the sodium sulfite solution (1.67 mL/s in this work); M is the concentration of the sodium sulfite solution (50 mol/m^3); and 2 is stoichiometry in the reaction; V is the liquid volume (94 L in this work).

At the steady state, the dissolved oxygen concentration C is constant, which results in dC/dt becomes zero. The mass transfer coefficient can be calculated that:

$$k_La = QM/[2VC^*(1 - C/C^*)] \quad (3)$$

The experimental results are reproducible, with an average relative error of less than 10% after two- or three-time repeats. All the experimental results were done under non-flooding conditions.

3. Power Consumption Measurement

Power consumption of impellers can be calculated based on shaft torque installed between the impeller shaft and the motor bearings when the impeller system is rotating. The shaft torque was measured using a torque sensor (AKC-205, Chinese Academy of Aerospace Aerodynamics, China), and the underlying principle used is as follows:

$$J = K(v_l - v_{ul}) \quad (4)$$

where J stands for the torque of a shaft (N·m); K is the coefficient of a torque sensor ($N \cdot m \cdot A^{-1}$). v_l (A) is the current intensity under loaded and v_{ul} (A) is the current intensity under idle condition. The signal from the torque sensor was logged and transferred by a digital recorder to a computer. The digital signal data was processed using a LabVIEW program, which calculated the power drawn by Eq. (5):

$$P = 2\pi NJ \quad (5)$$

P is the power drawn (W); N is the impeller rotation speed (s^{-1}).

4. Mass Transfer Correlations Fitting

Origin Pro 8 was used to fit the mass transfer correlations. The mass transfer rates are correlated in the dependency on impeller power consumption and superficial gas velocity as follows:

$$k_La = K_1 \cdot \left(\frac{P}{V}\right)^{K_2} \cdot (u_g)^{K_3} \quad (6)$$

The detailed data for correlations fitting are listed in Table 2.

5. Bubble Size Distribution Evaluation

The distribution of bubble size was analyzed based on transient pictures of the gas-liquid flow field taken by a high speed camera (PCO.1200S/hs, PCO, Germany). Three zones but not whole flow field were chosen: Zone 1 is located between impeller and liquid level (top); Zone 2 near the impeller (middle) and Zone 3 at the tank bottom (bottom). Only bubbles near the tank wall were measured. Details on the detect zones are shown in Fig. 4. To minimize optical refraction, the cylindrical tank was placed in a square tank. Because of bubbles seriously overlapping, bubbles have to be identified by vision and manually counted. The software of Image-Pro Plus 6.0 was employed for statistics on the number and size of bubbles. Bubbles have different shapes, mainly spherical and ellipsoidal. For ellipsoidal bubbles, the bubble effective equivalent diame-

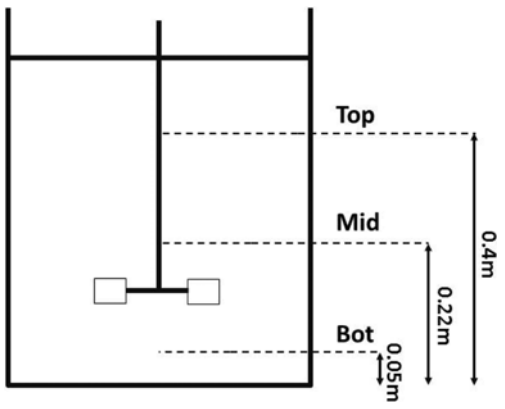

Fig. 4. Horizontal position of camera.

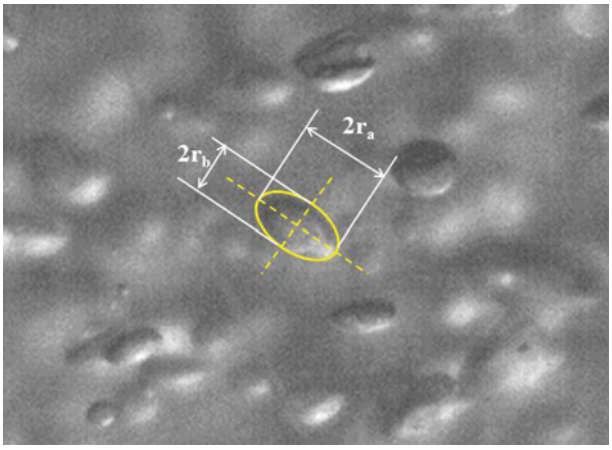

Fig. 5. Ellipsoidal bubble sampling.

ter listed in Eq. (7) was used to quantify the bubble size, as shown in Fig. 5 [26]. The statistical magnitude of bubbles was from 2000 to 3000 in every condition.

$$d_{eq} = 2\sqrt[3]{r_a^2 r_b} \tag{7}$$

RESULTS AND DISCUSSION

1. Mass Transfer Investigation of Single-impeller Configurations

1-1. Mass Transfer Performance of Single-impeller

The volumetric oxygen transfer capacities of eight single-impellers (Fig. 2) were investigated in this part. Fig. 6 shows that mass transfer rates of single-impeller become higher with increasing of impeller rotation speed and gas flow rate. At 200 rpm, the RT impeller gives the maximum value of k_La, which is 0.04 s^{-1}; CBY_N gives the minimum value, 0.0068 s^{-1}. At 300 rpm, the RT impeller also performs best with mass transfer rate of 0.062 s^{-1}; CBY_N produces the lowest value of 0.013 s^{-1}. It seems that the radial impellers works better than axial impellers in all the same impeller rotation speed and gas flow rate conditions, while the mixed flow impeller WH_{DU} stands between them. The differences between them become larger and larger as gas flow rate increases. This is caused by the different power-input between radial and axial impellers.

In this part, the data of impeller power per unit liquid volume and superficial gas velocity was fitted into equations for predicting mass transfer coefficient of different single-impellers. To compare

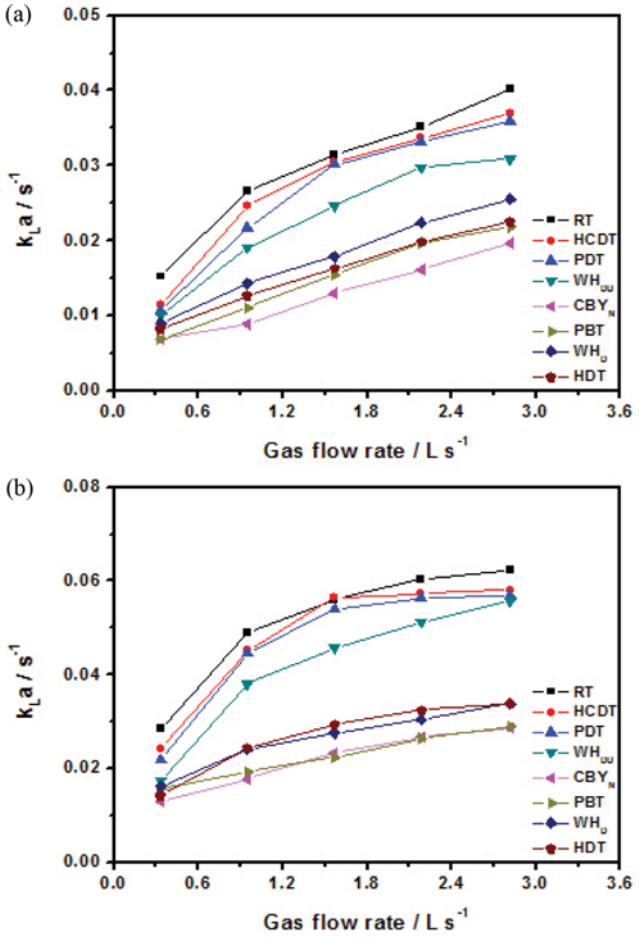

Fig. 6. Single impeller mass transfer rate ((a) N=200 rpm, (b) N=300 rpm).

the mass transfer performance of radial impellers and axial impellers, the equations were fitted as Eq. (8) and Eq. (9). For Eq. (8), the range of P/V is from 65 to 593 W/m^3 and the range of gas flow rate is from 0.2 to 1.8 vvm. For Eq. (9), the range of P/V is from 41 to 1,891 W/m^3 and the range of gas flow rate is from 0.2 to 1.8 vvm.

$$\text{Axial impellers: } k_La = 0.018 \times \left(\frac{P}{V}\right)^{0.44} (u_g)^{0.45},\ R^2 = 0.93 \tag{8}$$

$$\text{Radial impellers: } k_La = 0.02 \times \left(\frac{P}{V}\right)^{0.47} (u_g)^{0.48},\ R^2 = 0.98 \tag{9}$$

Table 3. Detailed information of referenced mass transfer correlations for single-impeller configuration

Reference	Mass transfer correlation	System	Description
van't Riet (1979)	$k_La = 2.6\times10^{-2}\times\left(\frac{P}{V}\right)^{0.4}(u_g)^{0.5}$	Water	Dynamic method; volume up to 2,600 L; 500<P/V<10,000 W/m^3; accuracy within 20%-40%
	$k_La = 2.0\times10^{-3}\times\left(\frac{P}{V}\right)^{0.7}(u_g)^{0.2}$	Electrolytes (Strong ionic solutions)	Dynamic method; 2<V<4,400 L; 500<P/V<10,000 W/m^3; accuracy within 20%-40%
Linek et al. (1987)	$k_La = 4.95\times10^{-3}\times\left(\frac{P}{V}\right)^{0.593}(u_g)^{0.4}$	Water	Steady-state method; 20 L reactor; superficial gas velocity of 0.212 and 0.424 cm/s; impeller rotation speed from 4.17 to 14.17 s^{-1}
	$k_La = 1.35\times10^{-3}\times\left(\frac{P}{V}\right)^{0.946}(u_g)^{0.4}$	Electrolytes (Strong ionic solutions)	

In this section, the mass transfer correlations we obtained are compared with that published by van't Riet [1] and Linek et al. [22]. The detailed information of referenced empirical correlations is listed in Table 3.

Some studies [27,28] have shown that transition concentration of sodium sulfate for bubble coalescence is 50 mol/m^3. The concentration of Na_2SO_4 solution in the stirred tank was kept below 2 mol/m^3 during all the experiments of this work. Although the solution is not a complete non-coalescing system, a certain proportion of bubbles will also be broken [29]. To have a comprehensive under-

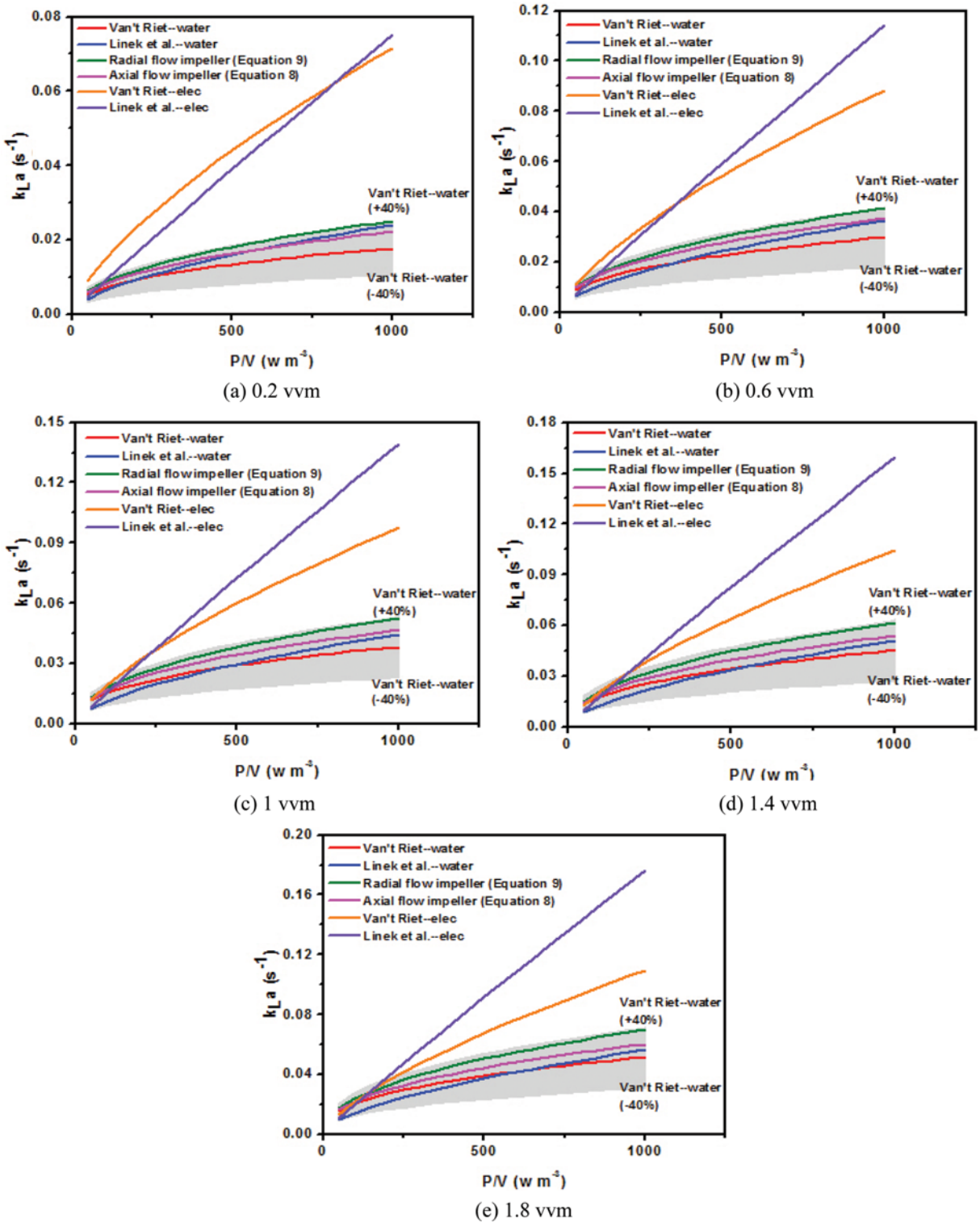

Fig. 7. Mass transfer empirical correlations comparison of single-impellers (gray area indicating ±40% error range of van't Riet's equation for coalescence system).

standing of the results, the data in this work were compared with referenced data obtained both in non-coalescent and coalescent systems. Fig. 7 shows the results in this work are much lower than referenced data of non-coalescent system, while close to data of water system. Nguyen et al. [29] found the percentage of bubble coalescence is around 90% when salt concentration is below 2 mol/m^3. Thus, the system of this work is much closer to a coalescent system.

Linek et al. [22] found that the mass transfer rate measured by the steady-state method is higher than the results of some dynamic method with the same power dissipation level. Gezork et al. [30] also found this phenomenon. This may be due to differences between steady-state and some dynamic methods. The steady state method does not ignore the effects of small bubbles [21]. The data collected by van't Riet is all mostly from the dynamic method, so it's reasonable that the mass transfer rate predicted by van't Riet is lower than the equation of Linek et al. if the power input is above 500 W/m^3. As for dynamic methods, the only case in which there is no need to resort to models for the behavior of the gas phase is when a pure gas is absorbed in a completely de-gassed liquid [23].

With the same volumetric power input, Eq. (8) and Eq. (9) fitted by steady-state method in this article also get higher k_La than the equations for water system of van't Riet and Linek et al. with the same power dissipation level. This is probably due to the presence of a small amount of sodium sulfate in the solution, which causes a small number of bubbles broken. Only at 0.2 vvm, the k_La calculated from Linek's equation (water) are higher than the value of axial impeller equation (Eq. 8). The k_La value calculated from Eq. (8) and Eq. (9) is still in the error range of van't Riet (water). The biggest difference of k_La value between radial impeller equation (Eq. (9)) and van't Riet (water) at 0.2 vvm is 41%; 0.6 vvm 37%; 1 vvm 37%; 1.4 vvm 37%; 1.8 vvm 36%. The radial impellers have higher mass transfer performance than the axial impellers. Zhu et al. [11] also reported that radial flow impellers show slightly higher mass transfer rate than the axial flow impellers up to 17% for a given specific power and gas flow rate. With power consumption increasing, the difference between radial and axial impellers is growing. The biggest difference of 16% appears in the condition of 1.8 vvm and 1,000 W/m^3. These results show that the mass transfer performance of radial impellers is better than axial impellers. This is because radial flow impellers have better gas handling capacity and can produce higher shear for breaking bubbles.

1-2. Bubble Size Distribution

Table 4. Parameters of HCDT and HDT

Impeller type	HCDT	HDT
Rotation speed (rpm)	200	300
Gas flow rate (L/s)	0.99	0.99
k_La (s^{-1})	0.025	0.024
P (W)	30.44	24.87
P/k_La (W·s)	1218	1036
d_{10} (mm)-top	2.81	2.96
d_{10} (mm)-mid	2.72	3.12
d_{10} (mm)-bot	2.68	3.06

Bubble mean diameters in three domains of radial HCDT impeller and axial HDT impeller are displayed in Table 4. For P/k_La, HCDT impeller is higher than axial HDT impeller. As for average bubble size, HDT impeller produces larger bubbles than HCDT impellers in all three domains. Larger bubble diameter contributes to a relatively lower k_La. For the radial impeller (HCDT), the mean

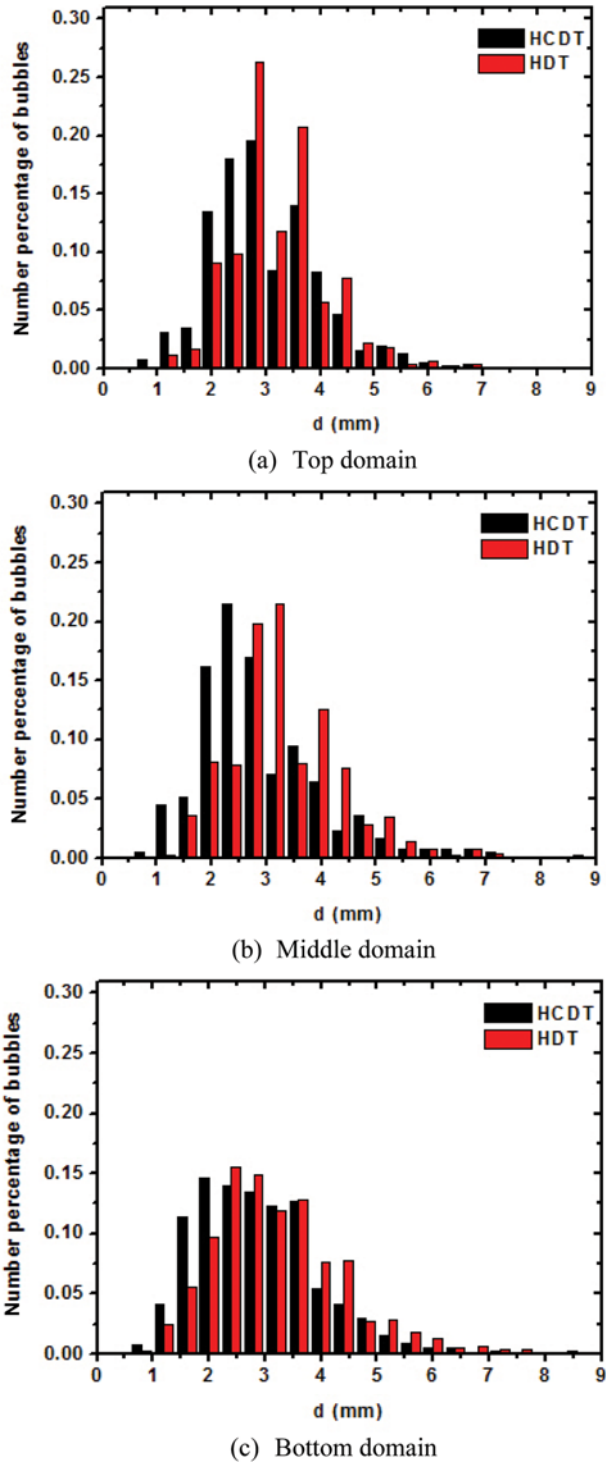

Fig. 8. Bubble distribution of HCDT and HDT ((a) Top domain, (b) middle domain, (c) bottom domain).

bubble diameter in the bottom is smallest, and no obvious bubble enlargement seems to occur along the up-flowing bubble path. Busciglio et al. [31] also found this phenomenon with a novel experimental technique based on advanced image processing coupled with experimental set-ups typically available for particle image velocimetry.

Bubble size distribution of HCDT impeller and HDT impeller at three different liquid levels is shown in Fig. 8. The size ranges for the bubble diameter histogram bins are from 0.4 mm to 9 mm. Distribution shapes of bubble size are positively skewed, in agreement with the previous work of Busciglio et al. [31]. Distribution trends of bubble diameter are almost the same in the top domain. Two peaks are seen for both kinds of impellers. The first and maximum peak appears around 2.8 mm, the second and relatively lower peak appears around 3.6 mm. HDT impellers have higher peaks at both sites than HCDT impeller. The proportion of bubbles with diameter smaller than 2.8 mm is larger for HCDT impeller than HDT impeller, which corresponds to smaller bubble size for HCDT. Distribution trends of bubble diameter in the middle domain are also similar for HCDT and HDT, a relatively higher peak is seen for each kind of impeller. Bubbles with diameter from 1.96 to 2.76 mm account for largest proportion for HCDT impeller, while most bubbles distributed from 2.76 to 3.16 mm for HDT impeller. In the bottom of the tank, bubble distribution patterns for two kinds of impeller are similar as well, except a peak appears slightly to the left for HCDT impeller. As a result, the equivalent effective diameter of most bubbles for HCDT impeller is smaller than HDT impeller.

2. Mass Transfer Investigation of Double-impeller Configurations

Fig. 9 shows the mass transfer rates of three double-impeller configurations (RT+RT, RT+WH_D and WH_D+WH_D) under several impeller rotation speeds and gas flow rates. It's clear that the RT+RT combination exhibits the highest mass transfer rates under all operating conditions, while WH_D+WH_D shows the lowest under all conditions. At 100 rpm, the difference between RT+RT, RT+WH_D and WH_D+WH_D is not obvious. At 200 rpm, the difference increases between three combinations. k_La range of RT+RT is from 0.02 s^{-1} to 0.049 s^{-1}; RT+WH_D from 0.02 s^{-1} to 0.044 s^{-1}; WH_D+WH_D from 0.018 s^{-1} to 0.038 s^{-1}. At 300 rpm, k_La range of RT+RT is from 0.03 s^{-1} to 0.079 s^{-1}; RT+WH_D is from 0.03 s^{-1} to 0.072 s^{-1}; WH_D+WH_D is from 0.03 s^{-1} to 0.06 s^{-1}. The power consumption of three double-impeller configurations is much different at the same impeller rotation speed, which is the main reason for the difference in mass transfer rates.

To compare the mass transfer rates of three double-configurations under the same power consumption, the mass transfer empirical correlations of double-impellers were fitted, which are listed in Eq. (10), Eq. (11) and Eq. (12). The range of gas flow rates is from 0.2 to 1.8 vvm for these three equations. As for Eq. (10), the range of P/V is from 87 to 2,923 W/m^3. For Eq. (11), the range of P/V is from 80 to 1,540 W/m^3. For Eq. (12), the range of P/V should be from 50 to 1,226 W/m^3.

$$\text{RT+RT: } k_La = 0.026 \times \left(\frac{P}{V}\right)^{0.5} (u_g)^{0.58},\ R^2 = 0.98 \quad (10)$$

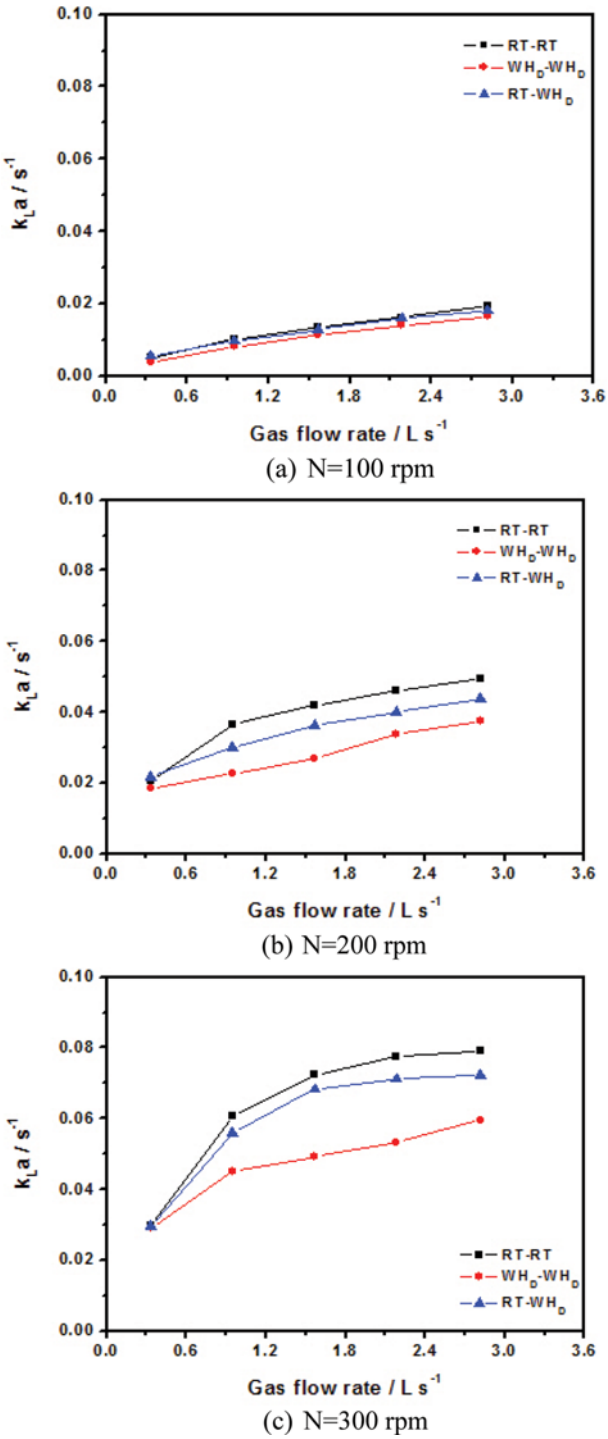

Fig. 9. Double-impeller mass transfer rate ((a) N=100 rpm, (b) N=200 rpm, (c) N=300 rpm).

$$\text{RT+WH}_D\text{: } k_La = 0.018 \times \left(\frac{P}{V}\right)^{0.53} (u_g)^{0.53},\ R^2 = 0.97 \quad (11)$$

$$\text{WH}_D\text{+WH}_D\text{: } k_La = 0.01 \times \left(\frac{P}{V}\right)^{0.59} (u_g)^{0.47},\ R^2 = 0.99 \quad (12)$$

Comparison of empirical correlations for gas-liquid mass transfer rate of double-impeller configurations is discussed in this sec-

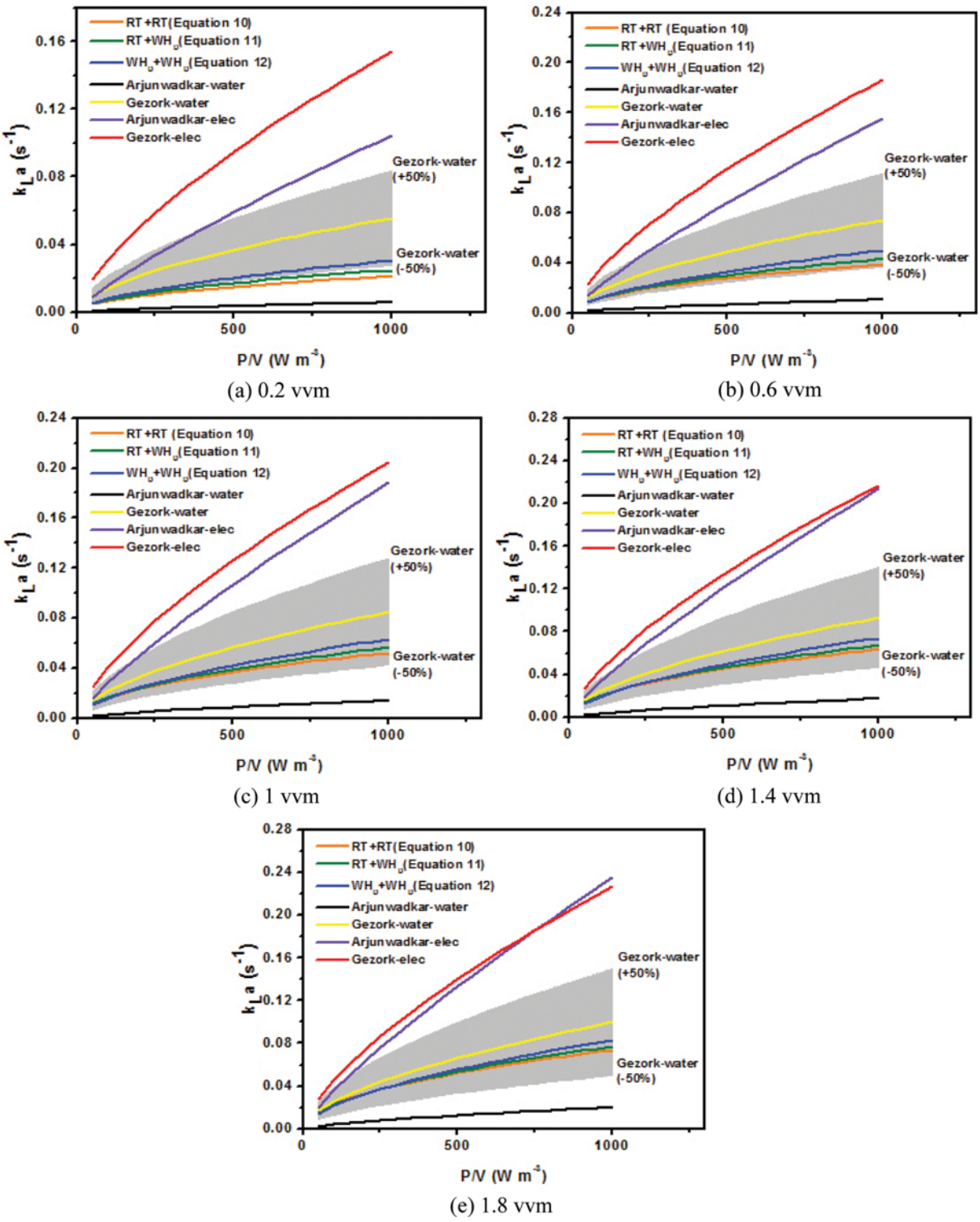

Fig. 10. Mass transfer empirical correlations comparison of double-impellers (gray area indicating ±50% error range of Gezork's equation in water system).

tion. The comparison of these results was all under non-flooding conditions. The black and purple lines in Fig. 10 represent the correlations of Arjunwadkar et al. [32], and dynamic method was employed in their work. The yellow and red lines represent the correlation correlations of Gezork et al. [30], who employed the steady-state method. The detailed information of referenced mass transfer correlations for double-impeller configurations is in Table 5.

Fig. 10 shows that results obtained in this work are far lower that the data obtained in the non-coalescence system, because the system of this work is much closer to the coalescent system as men-

Table 5. Detailed information of referenced mass transfer correlations for double-impeller configuration

Reference	Mass transfer correlation	System
Arjunwadkar et al. (1998)	$k_La = 2.04\times10^{-3}\times\left(\frac{P}{V}\right)^{0.68}(u_g)^{0.58}$	Water
	$k_La = 3.96\times10^{-3}\times\left(\frac{P}{V}\right)^{0.85}(u_g)^{0.38}$	Electrolytes (Strong ionic solutions)
Gezork et al. (2001)	$k_La = 5.3\times10^{-3}\times\left(\frac{P}{V}\right)^{0.59}(u_g)^{0.274}$	Water
	$k_La = 3.9\times10^{-3}\times\left(\frac{P}{V}\right)^{0.698}(u_g)^{0.182}$	Electrolytes (Strong ionic solutions)

Table 6. Correlations for prediction of gas-holdup [14]

Configuration	Gas-holdup correlation	Std. dev%
Single radial impeller	$\varepsilon_G = 0.01686\times\left(\frac{P}{V}\right)^{0.6241}(u_g)^{0.5669}$	13.1
Double radial impellers	$\varepsilon_G = 0.05051\times\left(\frac{P}{V}\right)^{0.4903}(u_g)^{0.5788}$	9.3
Single axial impeller	$\varepsilon_G = 0.04656\times\left(\frac{P}{V}\right)^{0.4666}(u_g)^{0.5816}$	9.5
Double axial impellers	$\varepsilon_G = 0.08193\times\left(\frac{P}{V}\right)^{0.5202}(u_g)^{0.7064}$	7.5

tioned above. Eq. (10), Eq. (11) and Eq. (12) are within the error limit of Gezork's equation (water). The error range of Gezork's correlation is up to 52.2%.

It is interesting that reverse results were found from the energy point of view. When gas flow rate is in the range from 0.2 vvm to 1.8 vvm, WH_D+WH_D performs best under the same power consumption and RT+RT is not as good as others. It can be seen from these results that double-axial flow impeller configurations have a better mass transfer performance. When designing and selecting double-impeller configurations, better mass transfer characteristics of double-axial flow impeller configurations should be considered.

3. Comparison between Single Impeller and Double Impeller

In this part, single-impeller configurations and double-impeller configurations are compared in terms of gas-liquid mass transfer performance. As mass transfer rate is related to gas-holdup, the gas-holdup correlations of Moucha et al. [14] are cited in Table 6.

Fig. 11 shows the comparison between single- and double-radial impellers. From energy consumption point of view, the single-impeller shows better mass transfer capacity than double-impeller configuration at gas flow rate of 0.2 vvm. While as gas flow flux increases to 1.8 vvm, the double-impeller configuration performs a little better. As for gas-holdup, the double-impeller configuration holds more gas than the single-radial impeller, and the difference grows with increasing gas flow flux.

The reverse trend exists for the axial impeller and its combination. Fig. 12 shows the comparison between the single- and double-axial impellers. Under all gas flow rates from 0.2 to 1.8 vvm, the double-axial configuration shows much higher k_La value with the same specific power consumption and higher gas-holdup than those of single-axial configuration.

CONCLUSIONS

Gas-liquid mass transfer characteristics of single-impeller and double-impeller were studied, including mass transfer rate, mass transfer performance and bubble size distribution. Different single-impeller configurations produced different mass transfer rates under the same operating conditions. At the same rotation speed and gas flow rate, radial flow impellers have the best mass transfer rates; mixed flow impeller comes next; axial flow impellers have the worst mass transfer capacity. From the mass transfer performance point of view, mass transfer rates of radial impellers will be gradually higher than axial impellers with power consumption increasing. Maximum difference between the empirical formula fitted in this work and that of van't Riet [1] is 40%, which is in the allowable error range. In terms of local bubble size distribution, the trend between radial flow impeller and axial flow impeller is similar to the same k_La value under a certain gas flow rate.

As for double-impeller configurations, mass transfer rates get higher with increasing rotation speed and gas flow rate. At 100 rpm, the three double-impellers have similar mass transfer capability. With increasing rotation speed, the RT+RT impeller has better mass transfer ability than the WH_D+WH_D impeller. The mass transfer performance of the axial double-impeller will be better than that of the radial double-impeller when power consumption gets higher. This result should be taken into account when selecting and designing the double impellers.

Mass transfer capability of double-impeller and single-impeller was also compared. At gas flow rate of 0.2 vvm, mass transfer rate of single radial impeller is higher than that of double radial impeller configuration under same power consumption. With the increase of the gas flow rate, the mass transfer performance of double radial

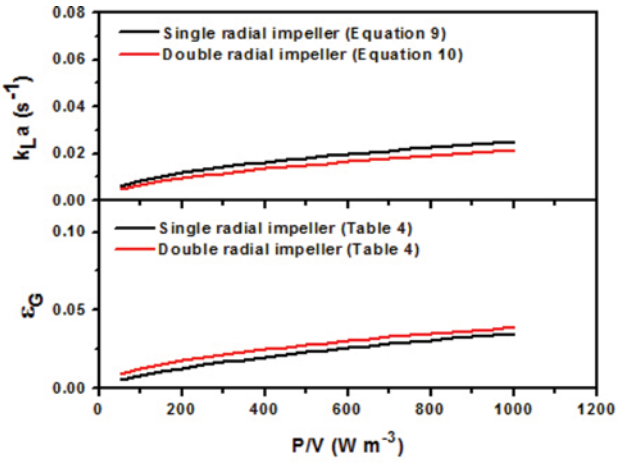

(a) 0.2 vvm

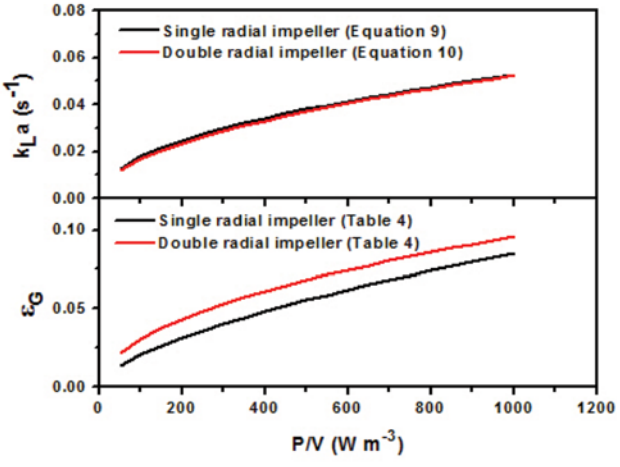

(b) 1 vvm

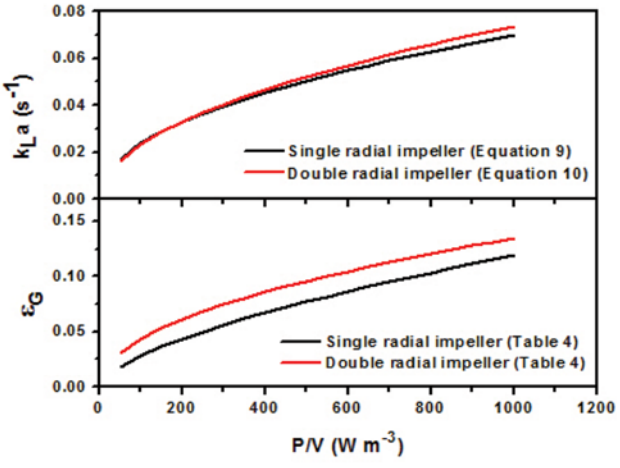

(c) 1.8 vvm

Fig. 11. Comparison of mass transfer and gas-holdup [14] between single- and double-radial impellers ((a) 0.2 vvm, (b) 1 vvm, (c) 1.8 vvm).

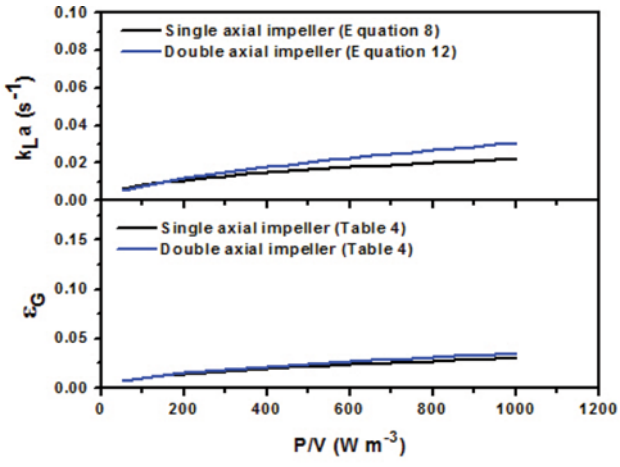

(a) 0.2 vvm

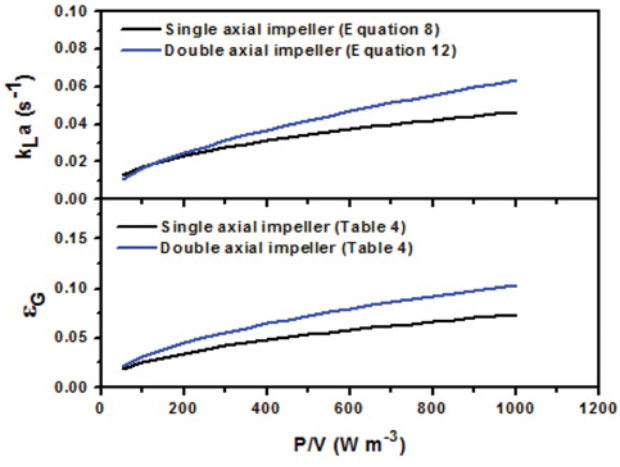

(b) 1 vvm

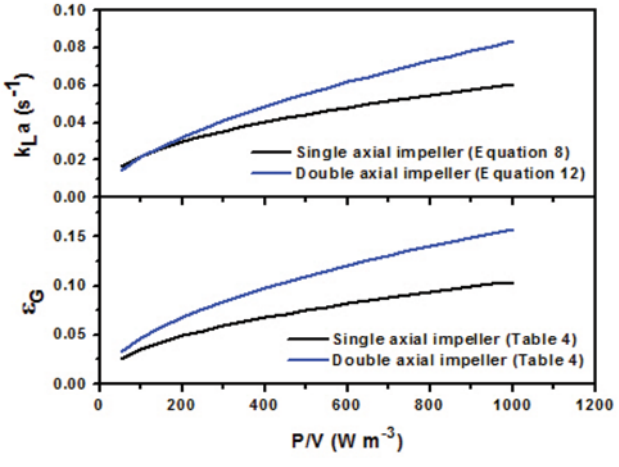

(c) 1.8 vvm

Fig. 12. Comparison of mass transfer and gas-holdup [14] between single- and double-axial impellers ((a) 0.2 vvm, (b) 1 vvm, (c) 1.8 vvm).

impeller configuration becomes better instead. For the axial impeller, the mass transfer performance of the double axial impeller is always better than that of the single axial impeller, no matter how much the gas flow rate is.

ACKNOWLEDGEMENT

The authors would like to acknowledge the support from Project 21506052 supported by National Natural Science Foundation

of China.

NOMENCLATURE

B : baffle width [m]
C^* : dissolved oxygen concentration at saturation [mol/m^3]
C : dissolved oxygen concentration [mol/m^3]
ΔC : impeller spacing [m]
C_d : bottom clearance of double-impeller [m]
C_s : bottom clearance of single-impeller [m]
C_{sp} : bottom clearance of sparger [m]
d : bubble diameter [mm]
d_{eq} : effective equivalent diameter [m]
d_{10} : bubble mean diameter [mm]
D_{im} : impeller diameter [m]
D_{sp} : sparger diameter [m]
D_t : tank diameter [m]
H_l : liquid height [m]
J : torque of a shaft [N·m]
k_La : volumetric mass transfer coefficient [s^{-1}]
K : coefficient of a torque sensor [N·m·A^{-1}]
K_1 : empirical constants in Eq. (6), dimensionless
K_2 : empirical constants in Eq. (6), dimensionless
K_3 : empirical constants in Eq. (6), dimensionless
M : concentration of the sodium sulfite solution [mol/m^3]
N : impeller rotation speed [s^{-1}]
P : power drawn [W]
P_b : oxygen probe clearance [m]
P_w : wall distance of oxygen probe [m]
Q : feeding rate of the sodium sulfite solution [m^3/s]
r : oxygen consumption rate [mol·m^{-3}·s^{-1}]
r_a : major axis of the ellipsoidal bubble [m]
r_b : minor axis of the ellipsoidal bubble [m]
S_{bubble} : bubble area in the picture [m^2]
t : time [s]
u_g : superficial gas velocity [m/s]
v_l : current intensity under loaded [A]
v_{ul} : current intensity under idle condition [A]
V : liquid volume [m^3]
ε_G : average gas-holdup (volumetric fraction of gas), dimensionless

REFERENCES

1. K. Van't Riet, *Ind. Eng. Chem. Process Des. Dev.*, **18**, 357 (1979).
2. M. K. Dawson, Ph.D Thesis, University of Birmingham, UK (1993).
3. M. J. Whitton and A. W. Nienow, The Proc 3rd Int Conf on Bioreactor and Bioprocess Fluid Dynamics, London (1993).
4. M. Cook, J. C. Middleton and J. R. Bush, The Proc 2nd Int Conf on Bioreactor Fluid Dynamics, Cranfield (1988).
5. A. W. Nienow, *Trans IChemE, Part A*, **74**, 417 (1996).
6. M. C. G. Warmoeskerken and J. M. Smith, *Chem. Eng. Res. Des.*, **67**, 193 (1989).
7. V. Linek, P. Benes and J. Sinkule, *Trans IChemE, Part C*, **69**, 145 (1991).
8. T. Martin, Ph.D Thesis, University of Birmingham, UK (1996).
9. T. Martin, C. M. McFarlane and A. W. Nienow, The Proc 8th Europ Mixing Conf, Rugby (1994).
10. Z. D. Chen and J. J. J. Chen, *Chem. Eng. Res. Des.*, **77**, 104 (1999).
11. Y. G. Zhu, P. C. Bandopadhyay and J.Wu, *J. Chem. Eng. Jpn.*, **34**, 579 (2001).
12. R. Sardeing, J. Aubin and C. Xuereb, *Trans IChemE, Part A*, **82**, 1589 (2004).
13. M. Bouaifi and M. Roustan, *Can. J. Chem. Eng.*, **76**, 390 (1998).
14. T. Moucha, V. Linek and E. Prokopová, *Chem. Eng. Sci.*, **58**, 1839 (2003).
15. T. Moucha, V. Linek, K. Erokhin, J. F. Rejl and M. Fujasová, *Chem. Eng. Sci.*, **64**, 598 (2009).
16. S. D. Shewale and A. B. Pandit, *Chem. Eng. Sci.*, **61**, 489 (2006).
17. A. J. Ungerman and T. J. Heindel, *Biotechnol. Prog.*, **23**, 613 (2007).
18. M. Fujasová, V. Linek and T. Moucha, *Chem. Eng. Sci.*, **62**, 1650 (2007).
19. M. Xie, J. Xia, Z. Zhou, J. Chu, Y. Zhuang and S. Zhang, *Ind. Eng. Chem. Res.*, **53**, 5941 (2014).
20. M. M. Buffo, L. J. Corrêa, M. N. Esperança, A. J. G. Cruz, C. S. Farinas and A. C. Badino, *Biochem. Eng. J.*, **114**, 130 (2016).
21. J. J. Heijnen, K. Van't Riet and A. J. Wolthuis, *Biotechnol. Bioeng.*, **22**, 1945 (1980).
22. V. Linek, V. Vacek and P. Beneš, *Chem. Eng. J.*, **34**, 11 (1987).
23. F. Scargiali, R. Russo, F. Grisafi and A. Brucato, *Chem. Eng. Sci.*, **62**, 1376 (2007).
24. V. Linek, P. Beneš, V. Vacek and F. Hovorka, *Chem. Eng. J.*, **25**, 77 (1982).
25. Y. Imai, H. Takei and M. Matsumura, *Biotechnol. Bioeng.*, **29**, 982 (1987).
26. G. Besagni, P. Brazzale, A. Fiocca and F. Inzoli, *Flow Meas. Instrum.*, **52**,190 (2016).
27. J. Zahradník, M. Fialová and V. Linek, *Chem. Eng. Sci.*, **54**, 4757 (1999).
28. C. P. Ribeiro Jr. and D. Mewes, *Chem. Eng. Sci.*, **62**, 4501 (2007).
29. P. T. Nguyen, M. A. Hampton, A. V. Nguyen and G. R. Birkett, *Chem. Eng. Res. Des.*, **90**, 33 (2012).
30. K. M. Gezork, W. Bujalski, M. Cooke and A. W. Nienow, *Chem. Eng. Res. Des.*, **79**, 965 (2001).
31. A. Busciglio, F. Grisafi, F. Scargiali and A. Brucato, *Chem. Eng. Sci.*, **102**, 551 (2013).
32. S. J. Arjunwadkar, K. Sarvanan, P. R. Kulkarni and A. B. Pandit, *Biochem. Eng. J.*, **1**, 99 (1998).